PNAS RESEARCH ARTICLE | CELL BIOLOGY

Fibrillin-1 regulates endothelial sprouting during angiogenesis

Florian Alonso[a,b], Yuechao Dong[a,b], Ling Li[c], Tiya Jahjah[a,b], Jean-William Dupuy[a], Isabelle Fremaux[a,b], Dieter P. Reinhardt[c,d,1], and Elisabeth Génot[a,b,1]

Edited by Brigid Hogan, Duke University, Durham, NC; received December 28, 2022; accepted April 20, 2023

Fibrillin-1 is an extracellular matrix protein that assembles into microfibrils which provide critical functions in large blood vessels and other tissues. Mutations in the fibrillin-1 gene are associated with cardiovascular, ocular, and skeletal abnormalities in Marfan syndrome. Here, we reveal that fibrillin-1 is critical for angiogenesis which is compromised by a typical Marfan mutation. In the mouse retina vascularization model, fibrillin-1 is present in the extracellular matrix at the angiogenic front where it colocalizes with microfibril-associated glycoprotein-1, MAGP1. In *Fbn1*$^{C1041G/+}$ mice, a model of Marfan syndrome, MAGP1 deposition is reduced, endothelial sprouting is decreased, and tip cell identity is impaired. Cell culture experiments confirmed that fibrillin-1 deficiency alters vascular endothelial growth factor-A/Notch and Smad signaling which regulate the acquisition of endothelial tip cell/stalk cell phenotypes, and we showed that modulation of MAGP1 expression impacts these pathways. Supplying the growing vasculature of *Fbn1*$^{C1041G/+}$ mice with a recombinant C-terminal fragment of fibrillin-1 corrects all defects. Mass spectrometry analyses showed that the fibrillin-1 fragment alters the expression of various proteins including ADAMTS1, a tip cell metalloprotease and matrix-modifying enzyme. Our data establish that fibrillin-1 is a dynamic signaling platform in the regulation of cell specification and matrix remodeling at the angiogenic front and that mutant fibrillin-1-induced defects can be rescued pharmacologically using a C-terminal fragment of the protein. These findings, identify fibrillin-1, MAGP1, and ADAMTS1 in the regulation of endothelial sprouting, and contribute to our understanding of how angiogenesis is regulated. This knowledge may have critical implications for people with Marfan syndrome.

fibrillin-1 | endothelial cell | angiogenesis | extracellular matrix proteins | Marfan Syndrome

Significance

Mutations in the gene coding for fibrillin-1, a protein in the extracellular matrix, cause Marfan syndrome, which is characterized by pathological changes in large blood vessels. We show that fibrillin-1 regulates angiogenesis, the formation of new blood vessels. A mouse model with a fibrillin-1 mutation associated with Marfan syndrome shows alterations in the vasculature of the retina of the eye. The angiogenesis defect can be corrected with a wild-type C-terminal fibrillin-1 fragment. These findings identify extracellular matrix proteins involved in angiogenesis and should benefit patients with Marfan syndrome.

Fibrillin-1 is an extracellular matrix (ECM) protein that assembles into microfibrils which provide critical functions in elastic tissues (1). Microfibrils are also found in the absence of elastin in tissues and organs including kidney, ciliary zonules of the eye, superficial regions of the skin, or the ear, where they typically intersect with basement membranes (2–4).

Mutations in the fibrillin-1 gene (*FBN1*) cause a spectrum of connective tissue disorders, including Marfan syndrome [MFS; Online Mendelian Inheritance in Man (OMIM) #154700]. MFS is associated with severe cardiovascular, skeletal, ocular, and adipose tissue defects (5, 6). Defective or reduced amounts of microfibrils affect the integrity of elastic tissues such as the aortic wall, leading to aneurysms and dissections (7). In addition, defective fibrillin-1-rich ciliary zonules cause ocular lens dislocation (8). However, individuals with MFS also present a reduction in the density of capillaries in the retina, whose etiology is entirely unknown (9, 10).

Fibrillin-1 is a large cysteine-rich extracellular glycoprotein with primarily tandem repeats of the calcium-binding epidermal growth factor–like (cbEGF) domain, and eight cysteine-containing transforming growth factor-beta (TGF-β)–binding protein–like (TB) domains. Monomers are arranged head to tail, forming a beads-on-a-string microfibril structure together with accessory proteins, including MAGP1 and 2, fibronectin, versican, perlecan, several fibulins, elastin, several ADAMTS proteins, and with integrins (11). Fibrillin-1 functions also as a repository for TGF-β and for several bone morphogenic proteins (BMPs) (12). Consequently, mutations affecting the structure, assembly, or stability of fibrillin-1 containing microfibrils impact their biochemical properties, cell–matrix interactions, cytokine bioavailability, or cell mechanosensing.

Murine models have been instrumental in advancing our understanding of MFS. Heterozygous mice with a substitution in a cbEGF domain in one allele (*Fbn1*$^{C1041G/+}$) reproduce several aspects of human MFS (13). The role of fibrillin-1 in the microvasculature has never been explored, and we therefore analyzed the consequences of the C1041G fibrillin-1 mutation in angiogenesis. We used the newborn mouse retina model in which retinal vascularization occurs postnatally and stereotypically. Guided by fibronectin and vascular endothelial growth factor-A (VEGF-A, thereafter VEGF) from astrocytes, the vascular network extends two-dimensionally across the retinal surface between P0 and P8.

Author contributions: E.G. designed research; F.A., Y.D., L.L., T.J., J.-W.D., I.F., and E.G. performed research; J.-W.D. and D.P.R. contributed new reagents/analytic tools; F.A., Y.D., L.L., T.J., I.F., and E.G. analyzed data; F.A. conceptualization, Methodology, Investigation, Visualization, Writing-Original Draft, Writing-Review & Editing; J.-W.D. mass spectrometry; D.P.R. conceptualization, Writing-Review & Editing, Funding Acquisition, Resources, Supervision; E.G. conceptualization, Methodology, Investigation, Writing-Original Draft, Writing-Review & Editing, Funding Acquisition, Resources, Supervision; and F.A., D.P.R., and E.G. wrote the paper.

Competing interest statement: F.A., D.P.R., and E.G. are listed as inventors on a patent describing the proangiogenic effects of hrFbn1-C reported in this manuscript. EP 4 019 035 A1 Novel recombinant fragments of fibrillin-1 and methods of use thereof, French patent application filed on behalf of UBx, INSERM, and McGill (McGill Reference #2021-024). Date of publication: June 29, 2022; Application number: 20217170.8; Date of filing: December 23, 2020; International Patent Classification (IPC): A61K 38/16 (2006.01), C07K 14/78 (2006.01), A61P 9/00 (2006.01), A61P 9/04 (2006.01), C12N 15/63 (2006.01), and A61P 9/10 (2006.01); Cooperative Patent Classification (CPC): A61K 38/16 and C07K 14/78. All other authors declare that they have no competing interests.

This article is a PNAS Direct Submission.

[1]To whom correspondence may be addressed. Email: dieter.reinhardt@mcgill.ca or elisabeth.genot@inserm.fr.

This article contains supporting information online at https://www.pnas.org/lookup/suppl/doi:10.1073/pnas.2221742120/-/DCSupplemental.

Published May 30, 2023.

In combination with yet unidentified signals, VEGF up-regulates the transmembrane Notch ligand Dll4 in angiogenic vessels and, most prominently, in the tip of endothelial sprouts (tip cells) (14). Dll4 activates the Notch1 receptor to induce proteolytic release of the Notch intracellular domain (NICD) that acts as a transcription factor, down-regulating VEGFR2/3 expression in adjacent cells (stalk cells) (14–16). In tip cells, low levels of Notch activity induce the formation of proteolytic podosomes that enable endothelial cell (EC) invasion (17). Stalk cells express another Notch ligand, Jagged-1 (18, 19), which antagonizes Dll4/Notch1 signaling back to the tip cell (18). VEGF and Dll4/Notch1 signaling cooperate in a negative feedback loop that specifies endothelial tip and stalk cells to ensure adequate vessel branching and function (16). The stalk phenotype also depends on the integration of Smad1/5 signaling with that of Notch (20–23). Consequently, Smad1/5 phosphorylation must be repressed to establish tip cell specification and this is achieved through neuropilin-1 (NRP1) (24).

In the present study, we reveal a fibrillin-1-rich transient matrix at the angiogenic front, which plays a critical role in retinal neovascularization, regulating Notch and Smad1/5 signaling and matrix remodeling. We propose that defects caused by fibrillin-1 deficiency in this transient matrix alter balanced angiogenesis by preventing proper specification of tip and stalk cells. Supplying the growing vasculature of *Fbn1*$^{C1041G/+}$ mice with a C-terminal fragment of fibrillin-1 provides therapeutical benefit.

Results

Fibrillin-1 Is Present at the Angiogenic Front of the Developing Retinal Vasculature. We detected fibrillin-1 in the developing retinal vasculature by immunofluorescent staining of flat-mounted wild-type (WT) mouse retinas at P6. In endothelial marker isolectin B4 (IB4)–stained retinas, fibrillin-1 was associated with arterioles (25), but unexpectedly, also at endothelial sprouts headed by tip cells (Fig. 1*A* and *SI Appendix*, Fig. S1*A*). Fibrillin-1 was observed in the tip cell surroundings as well as along tip cell bodies and their projections (Movie S1 and Fig. 1 *B* and *C*). Elastin staining was absent from the sprouting area where fibrillin-1 is abundant but clearly detectable at arterioles (Fig. 1*D*) (25). In fibrillin-1 mutant mice, fibrillin-1 immunostaining at the angiogenic front was reduced by ~40 to 60% compared to WT mice (Fig. 1*E*), similar to arterioles (Fig. 1*F*) (25). Fibronectin, which regulates pericellular microfibril assembly and deposition (26), was detected ahead of the sprouting area, but also throughout the vasculature and at similar levels in mutant retinas vs. controls (*SI Appendix*, Fig. S1 *B–D*). Fibrillin-1 associated with elastin is well described in large arterial vessels, but the detection of fibrillin-1 without association of elastin and in a provisional matrix suggested an unidentified functionality of the protein, at the angiogenic front.

Fibrillin-1 Deficiency Reduces Developmental Angiogenesis in the Retina. Analysis of flat-mounted retinas revealed that both the vascular coverage of the retina and the radial extension of the network were reduced in *Fbn1*$^{C1041G/+}$ mice, as compared to WT littermates (Fig. 2*A*). At the angiogenic front, the density of capillaries, the number of sprouts, capillary branch points, and meshes also decreased in *Fbn1*$^{C1041G/+}$ mice. The reduction in vascular outgrowth toward the periphery was consistent with a migration defect (Fig. 2*B*). Tip cells use their filopodia to adhere to the matrix for cell migration and podosomes facilitate this process by degrading the BM during the sprouting, branching, and anastomosing steps of angiogenesis (17) (Fig. 2*C*). In mutant retinas, the number of tip cells and filopodia per vessel length was markedly decreased (Fig. 2*D*). We also observed a reduction in podosome density and podosome size (Fig. 2*E*). Collectively, these results show a reduction in the migration- and invasion-associated cytoskeletal structures that characterize tip cells, in the developing retinal vasculature of *Fbn1*$^{C1041G/+}$ mice.

The C1041G Mutation in Fibrillin-1 Affects EC Phenotype and Behavior. The low prominence of phenotypic characteristics of the tip cells suggested a differentiation defect. To test Notch signaling, we stained the retinas for the NICD effector, and we explored the expression patterns of Dll4 and Jagged-1 ligands that are critical positive regulators of tip cell formation and sprouting (18) (Fig. 3*A*). In *Fbn1*$^{C1041G/+}$ vs. control retinas, Dll4 staining in tip cells was decreased (Fig. 3*B*) and NICD signal intensity at the front was lower (Fig. 3*C*). Dll4 signaling in tip cells is known to increase Jagged-1 expression in stalk cells (18). The scattered staining of Jagged-1 along the stalks at the angiogenic front in WT mice (19) was globally decreased in *Fbn1*$^{C1041G/+}$ retinas (Fig. 3*D*). P-ERK1/2 staining intensity was decreased in *Fbn1*$^{C1041G/+}$ animals (*SI Appendix*, Fig. S2*A*). To explore the migration/invasion defect, we focused on ESM1 and NRP1 that both regulate filopodia extension. ESM1 is expressed by tip cells in response to VEGF and increases VEGF bioavailability by competing with it for fibronectin binding (27). NRP1 enables filopodia extension in fibronectin-stimulated EC (28). At the angiogenic front, ESM1 and NRP1 were reduced in *Fbn1*$^{C1041G/+}$ mice vs. control mice (Fig. 3 *E* and *F*). NRP1 controls EC sprouting downstream of Notch by repressing the stalk phenotype in tip cells (24). NRP1 represses Smad phosphorylation by TGF-β/BMP and therefore P-Smad1/5 is normally low in these cells (24). However, in *Fbn1*$^{C1041G/+}$ retinas, P-Smad1/5 was increased at the angiogenic front and more specifically in tip cells, but not at the plexus (Fig. 3*G*). Collectively, these results indicate impaired tip cell determination and altered VEGF/Notch and Smad signaling at the angiogenic front in retinas of *Fbn1*$^{C1041G/+}$ mice.

To explore how fibrillin-1 could contribute to tip/stalk cell specification, we examined the induction of Notch pathway–related proteins in response to VEGF, and Smad pathways in response to BMP9, in fibrillin-1-deficient ECs in vitro. In primary ECs (human microvascular endothelial cells, HMVECs) transfected with small interfering RNA (siRNA) targeting fibrillin-1 (*SI Appendix*, Fig. S2 *B* and *C*), the regulation of eNOS was altered consistent with the endothelial dysfunction and compromised eNOS signaling reported in the aorta of MFS mice (29) (*SI Appendix*, Fig. S2*D*). The expression level of inhibitory Smad6 was found higher in fibrillin-1-silenced cells. Interestingly, the induction of Dll4 in response to VEGF stimulation was reduced (Fig. 3*H*). This was not associated with decreased ERK1/2 phosphorylation (*SI Appendix*, Fig. S2*D*) as expected. However, ERK and JNK pathways are known to be altered when fibrillin-1 is mutated (30), and we confirmed these findings in fibrillin-1-deficient ECs in vitro (*SI Appendix*, Fig. S2*D*). Fibrillin-1 deficiency also enhanced basal and VEGF-induced phosphorylation of VEGFR3 (*SI Appendix*, Fig. S2*D*), possibly as a compensatory mechanism (14). In response to BMP9, the phosphorylation of Smad1/5 was more robust in fibrillin-1-deficient ECs, consistent with a role for fibrillin-1 in repressing Smad signaling (Fig. 3*I*). P-Smad2/3 was unchanged and HMVECs did not respond to TGF-β (Fig. 3*I*). Together, our in vivo and in vitro data point at a role for fibrillin-1 in establishing the tip cell phenotype by regulating the suppression of the Smad1/5 response downstream of Notch (24).

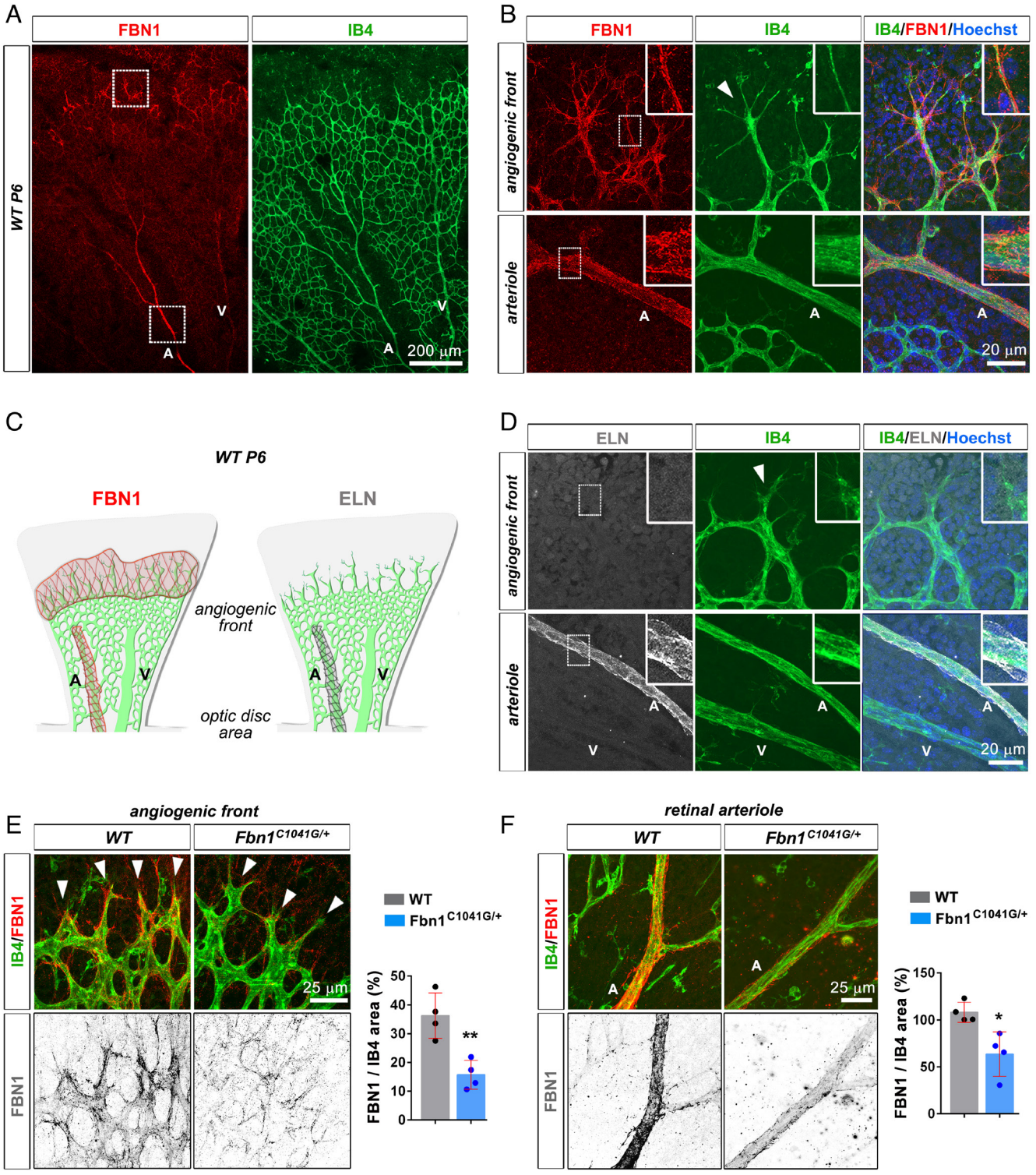

Fig. 1. Fibrillin-1 is expressed within the microvasculature of the developing mouse retina. (*A*) Fibrillin-1 (FBN1; red) and IB4 (green) staining in a petal of a flat-mounted P6 retina from a WT mouse. (*B*) High-magnification images from the boxed regions in *A*: angiogenic front (*Top*) and arterioles (*Bottom*): FBN1 (red), IB4 (green), and nucleus (blue), and at higher magnification in corresponding *Inset* (n = 10 WT mice). (*C*) Schematic representation of the FBN1 (red) and elastin (ELN; gray) localization in the vascular network (green). (*D*) IB4 (green)- and ELN (white)-stained retinal vessels, and at higher magnification in corresponding *Inset* (n = 3 WT mice). (*E*) IB4 (green)- and FBN1 (red)-stained angiogenic front at P6. *Bottom* panels show inverted FBN1 signals. Quantification of the FBN1-positive area over the IB4-positive area is shown (n = 4 WT, 4 *Fbn1*$^{C1041G/+}$ mice). (*F*) Same experimental setup as in *E* analyzed at the level of arterioles. White arrowheads; tip cells, A; arteriole and V; venule. *$P < 0.05$; **$P < 0.01$ vs. WT mice (Student's *t* tests).

MAGP1 Regulates VEGF/Notch and BMP9 Responses. Fibrillin-binding MAGPs have been shown to regulate TGF-β/BMP signaling through direct binding (31). MAGPs, which interact with EGF-like repeats of fibrillins (32), can also interact with EGF-like repeats of Notch1 and ligands, leading to the activation of Notch signaling through noncanonical pathway (33). Thus, MAGPs could also be involved in tip cell specification through Smad and Notch pathways. MAGP1 has a wider tissue distribution than MAGP2 and is a constituent protein of microfibrils (33, 34). In the WT retina, both proteins

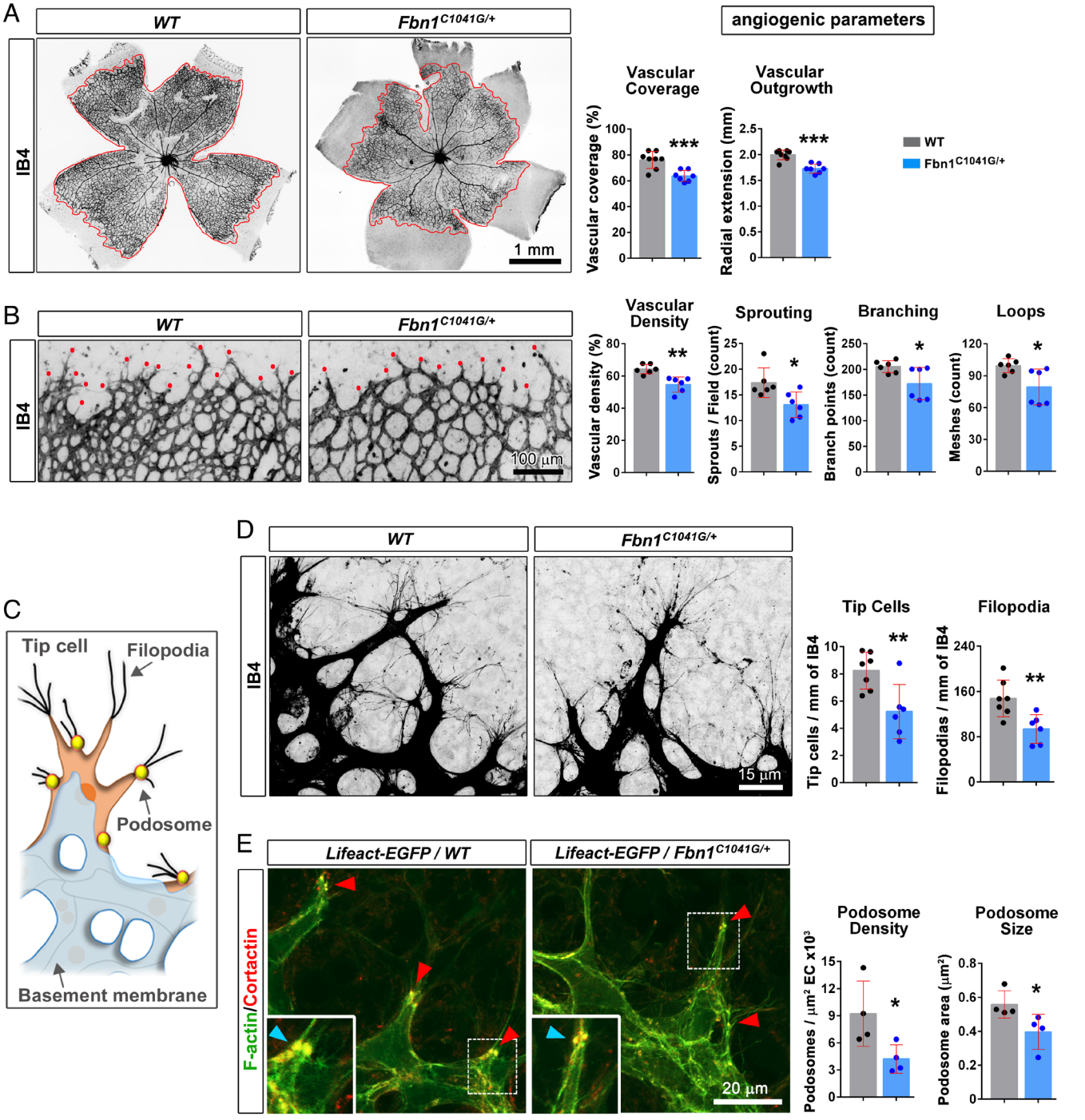

Fig. 2. A missense mutation in fibrillin-1 impacts neoangiogenesis in the developing mouse retina. (*A*) IB4 (black)-stained retinal whole mounts from P6 *Fbn1*$^{C1041G/+}$ and WT mice. Quantifications of the vascular coverage (area delineated by the red line) and the radial extension are shown. (n = 8 WT, 7 *Fbn1*$^{C1041G/+}$ mice). (*B*) Higher magnification images at the angiogenic front from P6 WT and *Fbn1*$^{C1041G/+}$ retinas. Quantitative assessments of the capillary density, the number of vascular sprouts (red dots), and the number of branch points and meshes (n = 6 WT, 6 *Fbn1*$^{C1041G/+}$ mice). (*C*) Schematic representation of a tip cell at the angiogenic front equipped with filopodia and podosomes. (*D*) High-resolution images of tip cells in P6 WT and *Fbn1*$^{C1041G/+}$ retinas. Quantification of tip cells and filopodia per vessel length (n = 7 WT, 6 *Fbn1*$^{C1041G/+}$ mice). (*E*) Representative images of the vascular front of WT and Lifeact-EGFP/*Fbn1*$^{C1041G/+}$ retinas labeled for cortactin (red)/F-actin (Lifeact-EGFP, green). Tip cell podosomes (red arrowheads) are highlighted by F-actin/cortactin colocalization, shown at higher magnification in the *Insets* (blue arrowheads). Quantitative analyses of podosome density and podosome area (n = 4 Lifeact-EGFP/WT, 4 Lifeact-EGFP/*Fbn1*$^{C1041G/+}$ mice). **P* < 0.05; ***P* < 0.01; ****P* < 0.001 vs. WT mice (Student's *t* tests).

were detected (Fig. 4*A* and *SI Appendix*, Fig. S3 *A–F*). MAGP2 staining was closely associated and evenly distributed along the vasculature (*SI Appendix*, Fig. S3 *D* and *E*). In contrast, MAGP1 staining was more prominent in the fibrillin-1-enriched area of the angiogenic front (Fig. 4*A* and *SI Appendix*, Fig. S3 *A* and *C*). MAGP2 staining was not different between *Fbn1*$^{C1041G/+}$ and WT retinal vasculature (*SI Appendix*, Fig. S3*F*), whereas MAGP1 immunostaining was weaker in *Fbn1*$^{C1041G/+}$ retinas and its pattern matched that of fibrillin-1 (Fig. 4*A* and *SI Appendix*, Fig. S3*F*).

The association of fibrillin-1 with tip cells also occurred at angiogenic sites in other tissues. Immunostaining of mouse brain sections localized fibrillin-1 and MAGP1 specifically at tip cells sprouting in the cortex (*SI Appendix*, Fig. S4). Thus, this

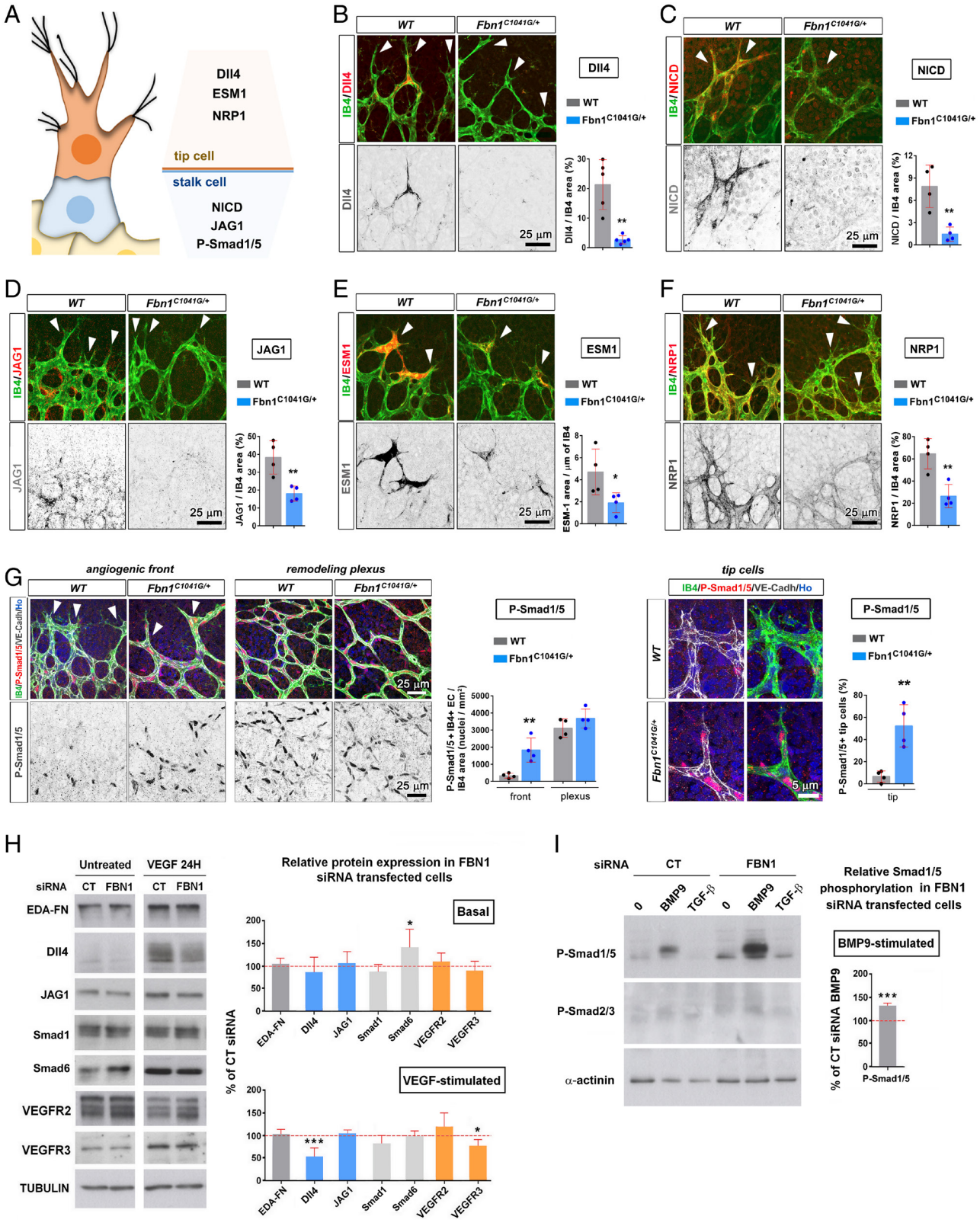

Fig. 3. Fibrillin-1 missense mutation impairs EC specialization. (*A*) Schematic representation of tip/stalk cell specification during sprouting angiogenesis. In response to VEGF, ECs differentiate into tip cells (orange) expressing ESM1, NRP1, and Dll4 markers. In adjacent stalk cells (blue), Dll4 from tip cells induces Notch intracellular cleavage (NICD). Stalk cells are also characterized by higher levels of JAG1 and P-Smad1/5. (*B*) IB4 (green)- and Dll4 (red)-stained angiogenic front from P6 *Fbn1*$^{C1041G/+}$ and WT retinas. *Bottom* panels (*B*–*G*) show inverted signals. Quantification of the Dll4-positive area over the IB4-positive area is shown (n = 5 WT, 5 *Fbn1*$^{C1041G/+}$ mice). (*C*–*F*) Same experimental setup as in *B* for IB4 (green) and NICD (red) in *C*; for IB4 (green) and JAG1 (red) in *D*; for IB4 (green) and ESM1 (red) in *E*; and for IB4 (green) and NRP1 (red) in *F* (n = 4 WT, 4 *Fbn1*$^{C1041G/+}$ mice). (*G*) Images of the angiogenic front and of the remodeling plexus from WT and *Fbn1*$^{C1041G/+}$ P6 retinas labeled for IB4 (green), P-Smad1/5 (red), VE-cadherin (white), and Hoechst (Ho, blue). P-Smad1/5 and IB4 double-positive ECs relative to the IB4-positive area are shown. Higher-magnification images of the vascular fronts reveal an increased number of P-Smad1/5-positive tip cells in *Fbn1*$^{C1041G/+}$ vs. WT retinas (n = 4 WT, 4 *Fbn1*$^{C1041G/+}$ mice). White arrowheads; tip cells, $*P < 0.05$; $**P < 0.01$ vs. WT mice (Student's *t* tests). (*H*) Protein expression in HMVECs after *FBN1* silencing, in the basal state and after 24 h VEGF stimulation. (*I*) P-Smad1/5 and P-Smad2/3 in *FBN1*-silenced HMVECs, in the basal state and after 30 min TGF-β or BMP9 stimulation. Mean values + SD from four independent experiments. $*P < 0.05$; $***P < 0.001$ vs. respective control siRNA. (Student's *t* tests).

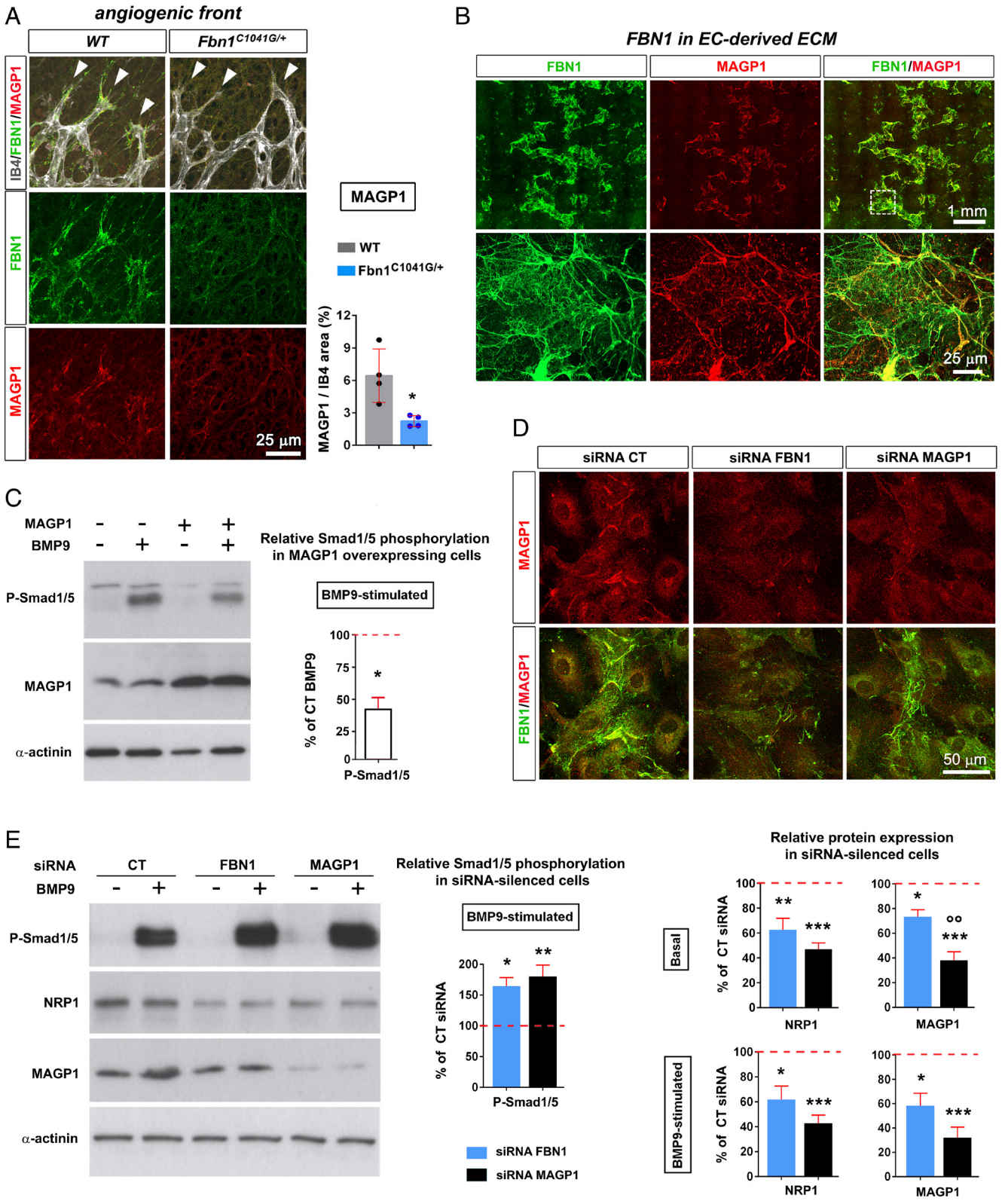

Fig. 4. MAGP1 deposition relies on fibrillin-1 expression and regulates Dll4, NRP1, and P-Smad1/5. (*A*) IB4 (white)-, FBN1 (green)-, and MAGP1 (red)-stained angiogenic front from P6 *Fbn1*$^{C1041G/+}$ and WT retinas. Quantification of the MAGP1-positive area over the IB4-positive area is shown. (n = 4 WT, 4 *Fbn1*$^{C1041G/+}$ mice). White arrowheads; tip cells, **P* < 0.05 vs. WT mice (Student's *t* tests). (*B*) FBN1 (green)- and MAGP1 (red)-stained decellularized ECM deposited by HMVECs. *Bottom* panels show higher-magnification images from corresponding *Inset*. (*C*) P-Smad1/5 in HMVECs overexpressing MAGP1, in the basal state (no detectable signal for P-Smad1/5) and after 30 min BMP9 stimulation. Mean values + SD from four independent experiments. **P* < 0.05 vs. BMP9-treated control cells. (Student's *t* tests). (*D*) FBN1 (green) and MAGP1 (red) double-stained *FBN1*- or *MAGP1*-silenced HMVECs. (*E*) Protein phosphorylation and expression in *FBN1*- or *MAGP1*-silenced HMVECs, in the basal state and after 30 min BMP9 stimulation. Mean values + SD from four independent experiments. **P* < 0.05; ***P* < 0.01; ****P* < 0.001 vs. respective control siRNA. °°*P* < 0.01 vs. *FBN1* siRNA (one-way ANOVA followed by Tukey's post-tests).

association of fibrillin-1 and MAGP1 with tip cells appears to be a more generalized feature of sprouting angiogenesis.

We therefore focused on MAGP1 which regulates Notch signaling cell autonomously (35). In HMVEC cultures, most of the MAGP1 staining was colocalized with fibrillin-1 in patches with the fibrillar matrix surrounding the cells (Fig. 4*B*). Although the spatiotemporal dynamics of tip/stalk cells is not replicated in vitro, feed-forward regulation on Notch signaling occurs. Notch activation up-regulates Dll4 expression, whereas Notch inhibition down-regulates Dll4 expression (36) and Notch inhibition up-regulates NRP1 expression (24). This was recapitulated in HMVECs using the Notch activator Yhhu-3792 and the Notch inhibitor DAPT (*SI Appendix*, Fig. S5 *A–C*). Interestingly, Yhhu-3792 increased the intracellular levels of fibrillin-1, whereas DAPT-treated cells appeared surrounded by extracellular fibrillin-1-positive fibrils (*SI Appendix*, Fig. S5 *D* and *E*).

Dll4 expression was indeed increased in HMVECs transfected with a plasmid-encoding MAGP1 (*SI Appendix*, Fig. S6). MAGP1 overexpression also reduced P-Smad1/5 upon BMP9 stimulation (Fig. 4*C*). Conversely, MAGP1-silenced cells responded more robustly to BMP9 than controls (Fig. 4 *D* and *E*). Smad1/5 phosphorylation was increased in a similar manner to fibrillin-1 silencing (Fig. 3*I*). Remarkably, NRP1 was down-regulated in the absence of MAGP1 and fibrillin-1 (Fig. 4*E*), consistent with a role for NRP1 in repressing BMP9 signaling (24).

Collectively, these data suggest overactivation of the Smad1/5 pathway in a fibrillin-1- and MAGP1-deficient microenvironment as a determinant of loss of tip cell capacity and sprouting.

A Recombinant Polypeptide Corresponding to the C-Terminal Half of Fibrillin-1 Displays Proangiogenic Properties. We used a recombinant C-terminal half of fibrillin-1 (hrFbn1-C) that is able to multimerize into bead-like structures (37), in an attempt to rescue the fibrillin-1 deficiency caused by the *Fbn1*^{C1041G} mutation (Fig. 5*A*). We performed intravitreal injection of hrFbn1-C in the eye of *Fbn1*$^{C1041G/+}$ animals at P4 and allowed neovascularization until P6 (Fig. 5*B*). Angiogenesis was restored under these conditions (Fig. 5*C*). P-Smad1/5 and NRP1 staining returned to normal levels, suggesting that restoration of angiogenic parameters was indeed the result of restoration of tip cell identity (Fig. 5 *D* and *E*). MAGP1 staining was restored at the angiogenic front in hrFbn1-C-injected eyes (Fig. 5*F*). hrFbn1-C could be detected in the retina by immunolabeling of its histidine tag (*SI Appendix*, Fig. S7). When hrFbn1-C was added to ECs in culture, it was detected in the ECM, associated with endogenously secreted fibrillin-1 (*SI Appendix*, Fig. S8).

Collectively, at the angiogenic front, hrFbn1-C corrected all identified defects induced by the fibrillin-1 mutation.

To test the proangiogenic activity of hrFbn1-C, in vivo sprouting angiogenesis was simulated in an in vitro assay that mimics the context of tip-cell biogenesis (17). A Matrigel plug containing VEGF was placed in a culture dish, and HMVECs were seeded to form a monolayer around it (Fig. 6*A*) (38). At the monolayer–Matrigel interface, sprouts invaded the Matrigel and the process was stimulated by hrFbn1-C but not with the control fibrillin-1 fragment hrFbn1-N (Fig. 6*B*). Cells exposed to hrFbn1-C showed a robust tip cell phenotype with an increase in the number and size of podosomes (Fig. 6*C*) (39). Additional in vitro angiogenesis assays confirmed the proangiogenic effect of hrFbn1-C on EC sprouting and tubulogenesis (*SI Appendix*, Fig. S9). These results establish that ECs are targets for fibrillin-1 and its C-terminal moiety promotes cytoskeletal rearrangements and endothelial sprouting.

hrFbn1-C Regulates ADAMTS1 Expression Which Is Deficient in Marfan Mice. To delineate the mechanism by which hrFbn1-C rescues EC behavior, the proangiogenic potential conferred by hrFbn1-C was investigated by comparative proteomic profiling using label-free mass spectrometry of hrFbn1-C or VEGF-stimulated HMVECs. After a stringent data filtering, a total of 21 proteins were identified to be significantly regulated in hrFbn1-C-stimulated vs unstimulated cells, of which 16 were up-regulated and 5 were down-regulated (Fig. 6*D*). Among the proteins significantly regulated by VEGF, 5 (50%) were similarly regulated by hrFbn1-C (Fig. 6*D*): ADAMTS1 (A disintegrin and metalloproteinase with thrombospondin motifs-1), WDR37 (WD repeat-containing protein 37), FLT1 (vascular endothelial growth factor receptor 1), FABP4 (fatty acid–binding protein 4), and FRMD5 (FERM domain–containing protein 5) (Fig. 6 *E* and *F*). These proteins play a role during angiogenesis, cell cycle progression, or cell adhesion/migration. To extend the investigation further, we have chosen ADAMTS1, a secreted Zn^{2+}-dependent metalloprotease, due to its high score and because other isoforms in this family, ADAMTS6, ADAMTS10, and ADAMTS17, bind fibrillins and are matrix modifiers of fibrillin assembly or microfibril function (40). In the vascular system, ADAMTS1 is known as an endothelial tip cell–enriched gene regulated by VEGF/Notch signaling (41). Moreover, heterozygous ADAMTS1$^{+/-}$ mice phenocopy aortic aneurysmal disease caused by the fibrillin-1 C1041G mutation in mice, highlighting a role for ADAMTS1 in fibrillin-1 function (42).

To confirm mass spectrometry analyses, western blot analysis was performed on these samples (Fig. 6*G*). ADAMTS1 expression was up-regulated by VEGF as expected (43). hrFbn1-C-, but not hrFbn1-N, doubled ADAMTS1 protein levels, whereas no additive or synergistic effect was observed between the two stimuli.

These data point at a proangiogenic action carried out by hrFbn1-C, but not hrFbn1-N on EC sprouting (Fig. 6*B*). In the WT mouse retina, ADAMTS1 was detected in the fibrillin-1-enriched zone at the angiogenic front with a staining pattern indistinguishable from that of MAGP1 (Fig. 6*H*). ADAMTS1 and fibrillin-1 colocalized in the ECM around Dll4- or ESM1-positive tip cells (*SI Appendix*, Fig. S10). The two proteins also colocalized in the fibrillar matrix deposited by cultured ECs (*SI Appendix*, Fig. S11). In the *Fbn1*$^{C1041G/+}$ retina, the staining was weaker than that in control retinas, indicating that ADAMTS1 expression or/and attachment to the BM/ECM was impaired in mutant mice (Fig. 6*H*). In the rescue experiment, leading to the recovery of the WT phenotype, ADAMTS1 immunoreactivity was restored in hrFbn1-C-injected eyes of *Fbn1*$^{C1041G/+}$ animals (Fig. 6*H*).

The role of ÁDAMTS-1 at the angiogenic front during retinal vascularization has never been directly addressed. In fact, this metalloprotease is known to inhibit angiogenesis by sequestering VEGF and inducing the release of antiangiogenic peptides from the ECM and the BM constitutive component, thrombospondin1 (TSP1) (44). Immunostaining detected TSP1 around retinal vessels but it was absent from the tip cell protrusions where MAGP1, fibrillin-1, and ADAMTS1 are preferentially detected (*SI Appendix*, Fig. S12). Moreover, we found no significant difference in TSP1 vessel coverage between the retinas of WT and MFS mice (*SI Appendix*, Fig. S12). Another ADAMTS1 substrate in this environment is versican (45). This large chondroitin sulfate proteoglycan is incorporated in the BM by surrounding cells, covalently bound to fibrillin-1 (46), and actively processed during the early course of angiogenesis (43).

ADAMTS-mediated cleavage of versican generates an N-terminal DPEAAE fragment (versican V1) which associates with ECs. The

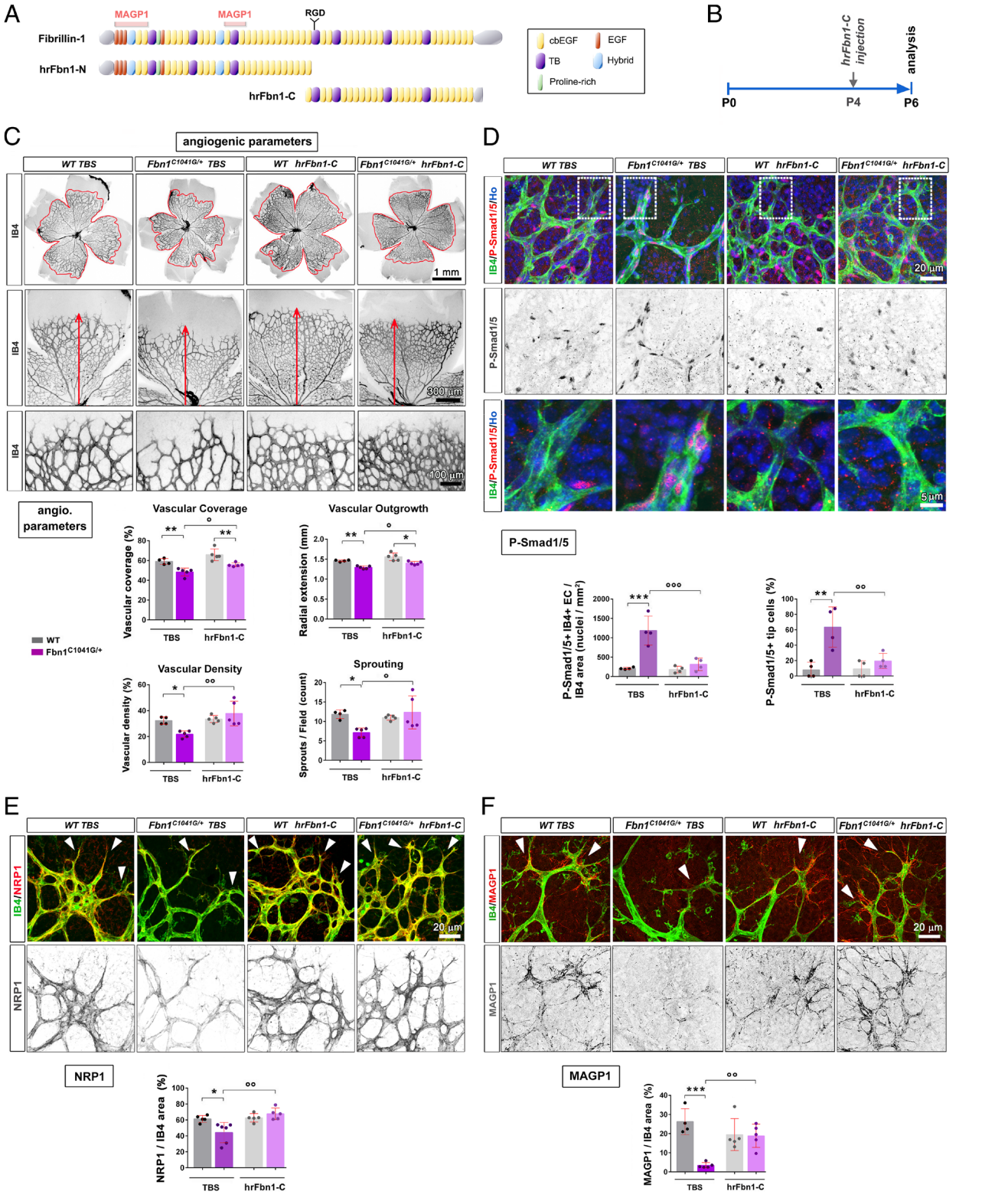

Fig. 5. A recombinant fibrillin-1 C-terminal polypeptide (hrFbn1-C) corrects the retinal vascular defects of *Fbn1*$^{C1041G/+}$ mice. (*A*) Schematic diagram of the full-length human FBN1 protein together with the recombinant polypeptides used in this study: hrFbn1-N and hrFbn1-C. Note that hrFbn1-C contains the only RGD motif in FBN1, while hrFbn1-N contains the two MAGP1-binding domains. (*B*) Schematic representation of the protocol of hrFbn1-C intravitreal injection into the eye at P4. Neovascularization was allowed until P6 and angiogenic parameters were assessed. (*C*) IB4 (black)-stained retinal whole mounts from WT and *Fbn1*$^{C1041G/+}$ mice injected with TBS or hrFbn1-C. Quantification and representative images of the vascular coverage (red line, *Top*), radial extension (red arrow, *Middle*), capillary density and sprouting (*Bottom*). (n = 4 TBS- and 5 hrFbn1-C-injected WT, and 5 TBS- and 5 hrFbn1-C-injected *Fbn1*$^{C1041G/+}$ mice). (*D*) IB4 (green)-, Hoechst (blue)-, and P-Smad1/5 (red)-stained angiogenic front from WT and *Fbn1*$^{C1041G/+}$ mice injected with TBS or hrFbn1-C. Quantification of P-Smad1/5 and IB4 double-positive ECs relative to the IB4-positive area is shown. Higher-magnification images of the vascular front (*Bottom*) reveal a decreased number of P-Smad1/5-positive tip cells in *Fbn1*$^{C1041G/+}$ injected with hrFbn1-C vs. TBS-injected *Fbn1*$^{C1041G/+}$ retinas (n = 4 TBS-injected WT; 4 hrFbn1-C-injected WT; 4 TBS-injected *Fbn1*$^{C1041G/+}$; 4 hrFbn1-C-injected *Fbn1*$^{C1041G/+}$ mice). (*E* and *F*) Same experimental setup as in *D* for IB4 (green) and NRP1 (red) in *E* (n = 5 TBS-injected WT; 5 hrFbn1-C-injected WT; 6 TBS-injected *Fbn1*$^{C1041G/+}$; 5 hrFbn1-C-injected *Fbn1*$^{C1041G/+}$ mice); for IB4 (green), MAGP1 (red) in *F* (n = 4 TBS- and 5 hrFbn1-C-injected WT and 5 TBS- and 5 hrFbn1-C-injected *Fbn1*$^{C1041G/+}$ mice). Quantification of NRP1 or MAGP1-positive areas over the IB4-positive area is shown. White arrowheads; tip cells. $*P < 0.05$; $**P < 0.01$; $***P < 0.001$ vs. respective WT mice. $°P < 0.05$, $°°P < 0.01$; $°°°P < 0.001$ vs. respective TBS-injected mice (two-way ANOVA followed by Tukey's post-tests).

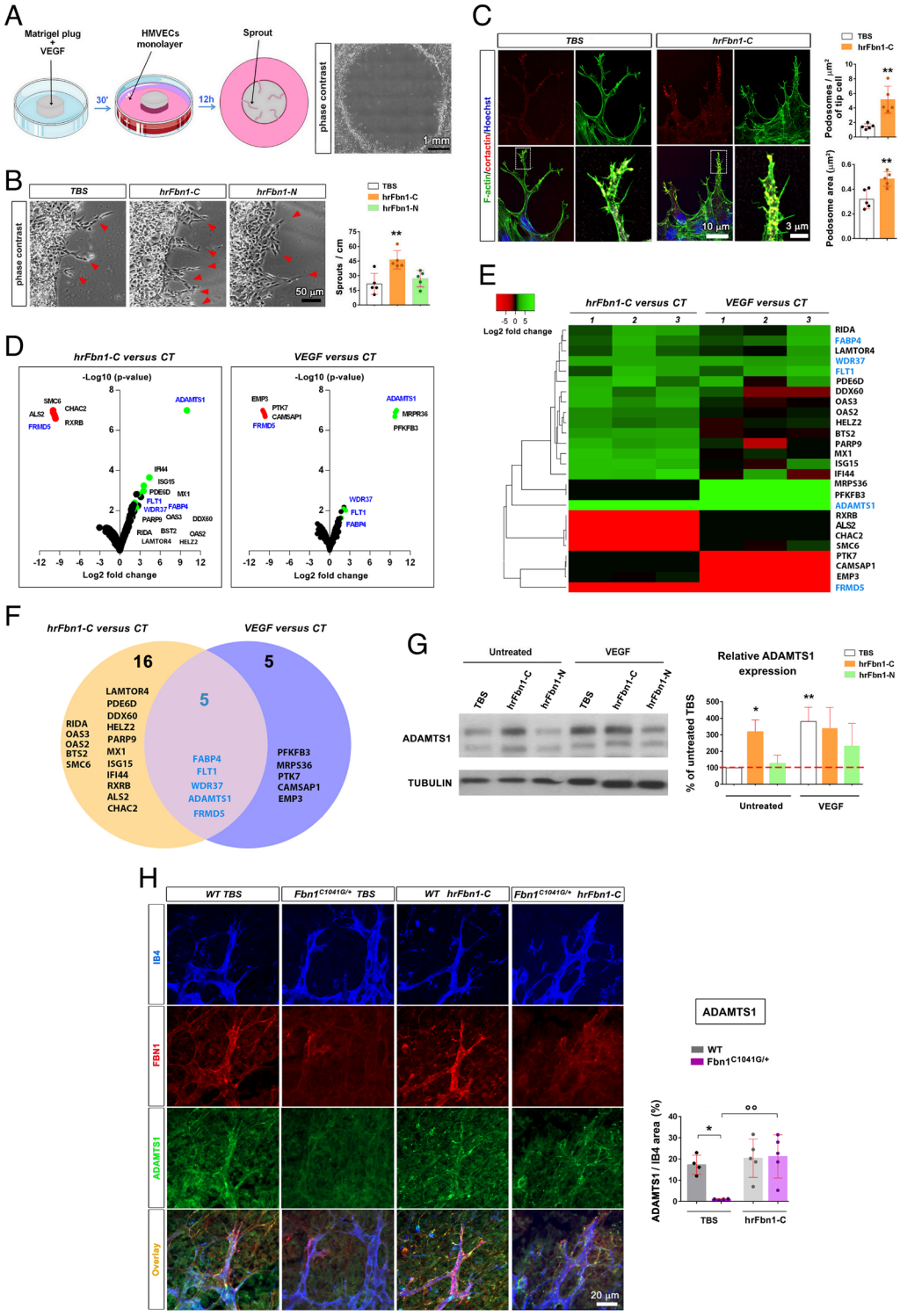

Fig. 6. hrFbn1-C displays proangiogenic properties. (*A*) Schematic representation of the in vitro angiogenesis invasion assay and phase-contrast microscopic image showing the tip-cell-like cell phenotype of HMVECs exposed to Matrigel+VEGF. (*B*) High-magnification phase-contrast images of HMVECs protruding into the Matrigel supplemented with either TBS, hrFbn1-C, or hrFbn1-N. Quantitative analysis of EC sprouting (red arrowheads) under the different conditions. $^{**}P < 0.01$ vs. TBS. (one-way ANOVA followed by Tukey's post-test). (*C*) F-actin (green)/cortactin (red) double staining of tip-cell-like ECs protruding into the Matrigel supplemented with either TBS or hrFbn1-C showing podosomes and protrusions, and higher-magnification images corresponding to the respective *Insets* (*Lower Right*). Quantitative analysis of podosome number and size. $^{**}P < 0.01$ vs. TBS. (Student's *t* tests). (*D*) Volcano plot [−log10(*P*-value) vs. log2(fold change)] showing protein expression changes in HMVECs stimulated for 24 h with either hrFbn1-C or VEGF vs. unstimulated cells (CT). Proteins were considered regulated significantly when found similarly regulated in the three biological replicates by two-sided Student's *t* tests with a *P*-value <0.05 (down-regulated proteins in red, up-regulated proteins in green). Proteins similarly regulated by hrFbn1-C and VEGF are highlighted in blue. (*E*) Heatmap of log2(fold change) following hierarchical clustering of significantly regulated proteins after hrFbn1-C or VEGF stimulation. For each protein, the log2(fold change) measured in the replicates (noted 1, 2, 3) is shown. (*F*) Venn diagram of all the proteins found to be significantly regulated by hrFbn1-C and/or VEGF. (*G*) ADAMTS1 expression levels after treatment of HMVECs with TBS, hrFbn1-C, or hrFbn1-N, in the basal state and after 24 h VEGF stimulation. Mean values + SD from four independent experiments. $^{*}P < 0.05$; $^{**}P < 0.01$ vs. respective TBS only–treated cells (two-way ANOVA followed by Tukey's post-test). (*H*) IB4 (blue)-, FBN1 (red)-, and ADAMTS1 (green)-stained angiogenic front from WT and *Fbn1*$^{C1041G/+}$ mice injected with TBS or hrFbn1-C. Quantification of the ADAMTS1-positive area over the IB4-positive area is shown (n = 4 TBS- and 5 hrFbn1-C-injected WT and 4 TBS- and 5 hrFbn1-C-injected *Fbn1*$^{C1041G/+}$ mice). $^{*}P < 0.05$ vs. respective WT mice. $^{\circ\circ}P < 0.01$ vs. respective TBS-injected mice (two-way ANOVA followed by Tukey's post-test).

fragment was preferentially detected at the angiogenic front where it colocalized in part with ADAMTS1 (*SI Appendix*, Fig. S13) and staining intensity was found much weaker in *Fbn1*$^{C1041G/+}$ mice (*SI Appendix*, Fig. S14). ADAMTS4 and ADAMTS5 which have a more potent versicanase activity than ADAMTS1 were not found associated with the retinal vasculature, nor enriched at the angiogenic front (*SI Appendix*, Fig. S15).

Altogether, the data show that hrFbn1-C rescues all identified deficiencies resulting from defective fibrillin-1 during vascularization of the retina in *Fbn1*$^{C1041G/+}$ mice.

Discussion

The production and breakdown of ECM plays a central role in angiogenesis (47). Here, we reveal a transient matrix containing fibrillin-1, MAGP1, and ADAMTS1 restricted to the angiogenic front during developmental angiogenesis.

Mutant Fibrillin-1 Impairs Tip/Stalk Cell Specification and Reduces Angiogenesis. Fibrillin-1 staining always coincided with the angiogenic front as it progressed, consistent with fibrillin-1-instructing cell behavior at this location and supported by the abnormalities of tip cells and signaling pathways when fibrillin-1 deposition was reduced. The emerging picture is that of an impaired VEGF/Notch and Smad signaling circuitry that prevents proper cell specification, resulting in less distinctive tip and stalk cell phenotypes.

In this situation where NICD and Dll4 are decreased, we explain the absence of excessive tip cell formation by the fact that NRP1 is down-regulated at tip cells in *Fbn1*$^{C1041G/+}$ retinas. NRP1 acts as a downstream effector of Notch, and Notch inhibition does not induce excessive tip cell formation in the absence of NRP1 (24). The absence of NRP1 may also account for the reduction of filopodia that typify tip cells because the protein is essential for their formation by enabling the ECM-induced activation of Cdc42 (28). The decrease in podosome size and number is consistent with an incomplete reduction of Notch activity in tip cells (17). NRP1 also contributes to positive feedback loops on VEGFR2 expression (48, 49) and VEGF bioavailability (50). NRP1 enables cell specification by inhibiting Smad1/5 phosphorylation in tip cells to repress the stalk cell phenotype (24). Accordingly, the reduction of NRP1 in cells at the angiogenic front is associated with increased P-Smad1/5 levels in *Fbn1*$^{C1041G/+}$ retinas. Our in vitro experiments show that a fibrillin-1 deficit in ECs impacts the regulation of Dll4, NRP1, and P-Smad1/5. As proper tip/stalk cell specification depends on integration of Notch and Smad1/5 signaling cascades (21–23), these in vitro results support the hypothesis that fibrillin-1 regulates sprouting angiogenesis.

Fibrillin-1 Mutation Is Associated with Reduced MAGP1 Deposition. MAGP1/2 directly interact with fibrillin-1 (32, 51) and regulate Notch signaling and TGF-β/BMP bioavailability (33). MAGP2, which in vitro promotes angiogenic cell sprouting by blocking Notch signaling in ECs through its ligand Jagged-1 (52), appeared as an attractive candidate in mediating the mutant fibrillin-1-induced angiogenesis defect. However, MAGP2 expression pattern was not restricted to the angiogenic front and was not altered by the fibrillin-1 C1041G mutation. In contrast, MAGP1 and fibrillin-1 staining more closely overlapped, and MAGP1 accumulation was decreased in the transient matrix at the angiogenic front in *Fbn1*$^{C1041G/+}$ retinas. The distinctive pattern of MAGP1 and MAGP2 localization supports distinct functions of the two proteins in retinal angiogenesis. MAGP1 interacts with EGF-like domains of Notch1 but regulates Notch independently of canonical ligands and this regulation, which occurs in cis, is therefore restricted to cells that express MAGP1 as shown in vitro (35). How MAGP1 interferes with Notch signaling in vivo is unknown. In vitro, silencing MAGP1 expression mimics the effects of fibrillin-1 loss in increasing P-Smad1/5 and reducing NRP1 expression in HMVECs. Conversely, overexpression of MAGP1 reduced P-Smad1/5 in vitro. MAGP1 may stimulate tip stalk shuffling, the process by which the tip cell is dynamically challenged and replaced by cells originating from the pool of stalk cells, in vivo.

Another mechanism by which MAGP1 might influence Smad1/5 signaling is through its ability to bind directly to BMPs, a scenario where fibrillin-1 and MAGP1 may work synergistically (31, 53–55). BMP9 is present at high concentrations in tissues and is a potent homeostatic factor. A reduction in MAGP1 deposition in mutant mice would therefore increase BMP9 availability. One MAGP1 binding site localizes close to the N terminus of fibrillin-1 (51), and a second one more centrally in the region of TB3-cbEGF11 (56). Interestingly, the C1041G mutation is located in cbEGF11, and thus could potentially alter fibrillin-1/MAGP-1 interaction. Our results support the hypothesis that fibrillin-1 together with MAGP1 is part of the transient matrix that contributes to tip cell specification at the angiogenic front. In addition, our studies reconcile the findings established by Fantin et al., which confer a key role for the matrix in the regulation of NRP1 signaling, with those of Aspalter et al., which confer a pivotal role for NRP1 in establishing differential responsiveness to BMP signaling (24, 28).

A Polypeptide Corresponding to the C-Terminal Half of Fibrillin-1 Has Proangiogenic Activities. Our data emphasize the role played by the ECM during angiogenesis. We highlight a proangiogenic effect of hrFbn1-C corresponding to the C-terminal half of fibrillin-1 which contains the sole RGD (Arg-Gly-Asp) integrin-binding site. Fibrillin-1 self-interaction sites are located close to the N- and the C-terminal ends (37) and hrFbn1-C is expected to interact with the N terminus of endogenous fibrillin-1. We have already observed the association of hrFbn1-C with fibrillin-1 secreted by ECs in culture. hrFbn1-C may therefore stabilize the interaction of MAGP1 at its N-terminal binding site (51) and the multimeric nature of hrFbn1-C may play a role in stabilizing mutant fibrillin-1 by preventing its degradation (37). hrFbn1-C may also provide more RGD sequences for integrin binding and thereby promote cell adhesion, signaling, and mechanosensing. The multimeric nature, the multiplicity of RGD sequences of hrFbn1-C, and/or the contribution of other proteins interacting with this portion of fibrillin-1 could thus account for its proangiogenic properties.

Fibrillin-1 Mutation Is Associated with Reduced ADAMTS1 Deposition Which Is Rescued by hrFbn1-C. We also detected ADAMTS1 in the transient matrix at the angiogenic front. As the function of this metalloprotease in tip cells is not known, we sought to explore its action on two of its substrates. While TSP1 at retinal vessels did not appear to be altered in MFS mice, versican processing was reduced. By proteolysis of versican, ADAMTS1 would modify the matrix to make it suitable for EC migration. Fibrillin-1 binds to ADAMTS6, ADAMTS10, and ADAMTS17 (40, 57), whether or not fibrillin-1 binds ADAMTS1 remains to be determined. Interestingly, ADAMTS1 was shown to inhibit Notch signaling and could thereby contribute to establish tip cell specification at the angiogenic front (58).

Our data establish that fibrillin-1 is a dynamic signaling platform in the regulation of cell specification and matrix remodeling at the angiogenic front and that mutant fibrillin-1-induced

defects can be rescued pharmacologically. Our in vivo experiments show that hrFbn1-C normalizes the transient matrix, including restoring MAGP1 and ADAMTS1 at the angiogenic front. Our in vitro experiments highlight that hrFbn1-C associates with endogenously secreted fibrillin-1, stimulates ADAMTS1 expression by ECs, but also regulates the expression of several other proteins. At present, we do not know whether hrFbn-1C exerts the same activity within the context of the full-length fibrillin-1 protein.

The association of different molecules that prime microfibril for specific tasks in various tissue contexts is likely tissue- and process-specific. Other fibrillin-1-interacting proteins may be involved in angiogenesis as well. While many pathological aspects in individuals with MFS are known for decades, retinal vascular pathophysiology was only described recently (9, 10). These studies show decreased retinal capillary vessel density in patients with MFS, correlating with aortic pathology. Since the *Fbn1*$^{C1041G/+}$ mice phenocopy the retinal vascular pathology of these patients, these mice are an excellent model to study the efficacies of relevant drugs to improve these microvascular defects.

Materials and Methods

Fbn1$^{C1041G/+}$ mice were provided by Hal Dietz (13). All procedures and protocols were conducted in accordance with the guidelines of the French Ministry of Health under the authority of the project Licenses #7313 and #19728. Details on animals and procedures are included in *SI Appendix*. *SI Appendix* also includes detailed Materials and Methods, including production of recombinant fibrillin-1 polypeptides, cell culture, transfection and stimulation, immunohistochemistry, western blot analysis, angiogenesis assays, label-free quantitative proteomics, and statistical analysis.

Data, Materials, and Software Availability. The mass spectrometry proteomics data have been deposited to the ProteomeXchange Consortium via the PRIDE partner repository (59) with the dataset identifier PXD029834. All other data are included in the article and/or supporting information. Materials generated in this study are available upon request.

ACKNOWLEDGMENTS. We warmly acknowledge Bob Mecham for the gift of elastin antibodies, Jean-Jacques Feige and Thomas Daubon for anti-TSP1 antibodies, and Hal Dietz for the gift of *Fbn1*$^{C1041G/+}$ mice. This research was funded by INSERM and the association "Marfans" (E.G.). Additional funding was from the Ligue contre le Cancer. F.A. was funded by the Berthe Fouassier-Eye Disease Foundation under the auspices of the Fondation de France and Fondation Lefoulon-Delalande. D.P.R. was supported by the Canadian Institutes of Health Research (PJT-162099), the Marfan Foundation, and the Glaucoma Foundation.

Author affiliations: [a]Université de Bordeaux F-33000 Bordeaux, France; [b]INSERM U1026, BioTis F-33000 Bordeaux, France; [c]Faculty of Medicine and Health Sciences, McGill University, Montreal, QC H3A 0C7, Canada; and [d]Faculty of Dental Medicine and Oral Health Sciences, McGill University, Montreal, QC H3A 0C7, Canada

1. B. A. Kozel, R. P. Mecham, Elastic fiber ultrastructure and assembly. *Matrix Biol.* **84**, 31–40 (2019).
2. W. Kriz, M. Elger, K. Lemley, T. Sakai, Structure of the glomerular mesangium: A biomechanical interpretation. *Kidney Int. Suppl.* **30**, S2–9 (1990).
3. M. Ohashi *et al.*, Histochemical localization of the extracellular matrix components in the annular ligament of rat stapediovestibular joint with special reference to fibrillin, 36-kDa microfibril-associated glycoprotein (MAGP-36), and hyaluronic acid. *Med. Mol. Morphol.* **41**, 28–33 (2008).
4. K. Tiedemann *et al.*, Microfibrils at basement membrane zones interact with perlecan via fibrillin-1. *J. Biol. Chem.* **280**, 11404–11412 (2005).
5. H. C. Dietz *et al.*, Marfan syndrome caused by a recurrent de novo missense mutation in the fibrillin gene. *Nature* **352**, 337–339 (1991).
6. D. M. Milewicz *et al.*, Marfan syndrome. *Nat. Rev. Dis. Prim.* **7**, 64 (2021).
7. P. N. Robinson *et al.*, The molecular genetics of Marfan syndrome and related disorders. *J. Med. Genet.* **43**, 769–787 (2006).
8. I. H. Maumenee, The eye in the Marfan syndrome. *Trans. Am. Ophthalmol. Soc.* **79**, 684–733 (1981).
9. H. Chen *et al.*, Characteristics of the foveal microvasculature in children with Marfan syndrome: An optical coherence tomography angiography study. *Retina* **42**, 138–151 (2022).
10. M. Di Marino *et al.*, Retinal and choroidal vasculature in patients with Marfan syndrome. *Transl. Vis. Sci. Technol.* **9**, 5 (2020).
11. A. R. F. Godwin *et al.*, The role of fibrillin and microfibril binding proteins in elastin and elastic fibre assembly. *Matrix Biol.* **84**, 17–30 (2019).
12. G. Sengle, L. Y. Sakai, The fibrillin microfibril scaffold: A niche for growth factors and mechanosensation? *Matrix Biol.* **47**, 3–12 (2015).
13. D. P. Judge *et al.*, Evidence for a critical contribution of haploinsufficiency in the complex pathogenesis of Marfan syndrome. *J. Clin. Invest.* **114**, 172–181 (2004).
14. R. Benedito *et al.*, Notch-dependent VEGFR3 upregulation allows angiogenesis without VEGF-VEGFR2 signalling. *Nature* **484**, 110–114 (2012).
15. M. Hellstrom *et al.*, Dll4 signalling through Notch1 regulates formation of tip cells during angiogenesis. *Nature* **445**, 776–780 (2007).
16. S. Suchting *et al.*, The Notch ligand Delta-like 4 negatively regulates endothelial tip cell formation and vessel branching. *Proc. Natl. Acad. Sci. U.S.A.* **104**, 3225–3230 (2007).
17. P. Spuul *et al.*, VEGF-A/Notch-induced podosomes proteolyse basement membrane collagen-IV during retinal sprouting angiogenesis. *Cell Rep.* **17**, 484–500 (2016).
18. R. Benedito *et al.*, The notch ligands Dll4 and Jagged1 have opposing effects on angiogenesis. *Cell* **137**, 1124–1135 (2009).
19. J. J. Hofmann, M. L. Iruela-Arispe, Notch expression patterns in the retina: An eye on receptor-ligand distribution during angiogenesis. *Gene Expr. Patterns* **7**, 461–470 (2007).
20. L. A. van Meeteren *et al.*, Anti-human activin receptor-like kinase 1 (ALK1) antibody attenuates bone morphogenetic protein 9 (BMP9)-induced ALK1 signaling and interferes with endothelial cell sprouting. *J. Biol. Chem.* **287**, 18551–18561 (2012).
21. A. Benn *et al.*, BMP-SMAD1/5 signaling regulates retinal vascular development. *Biomolecules* **10**, 488 (2020).
22. B. Larrivee *et al.*, ALK1 signaling inhibits angiogenesis by cooperating with the Notch pathway. *Dev. Cell* **22**, 489–500 (2012).
23. I. M. Moya *et al.*, Stalk cell phenotype depends on integration of Notch and Smad1/5 signaling cascades. *Dev. Cell* **22**, 501–514 (2012).
24. I. M. Aspalter *et al.*, Alk1 and Alk5 inhibition by Nrp1 controls vascular sprouting downstream of Notch. *Nat. Commun.* **6**, 7264 (2015).
25. F. Alonso, L. Li, I. Fremaux, D. P. Reinhardt, E. Genot, Fibrillin-1 regulates arteriole integrity in the retina. *Biomolecules* **12**, 1330 (2022).
26. L. Sabatier *et al.*, Fibrillin assembly requires fibronectin. *Mol. Biol. Cell* **20**, 846–858 (2009).
27. G. A. Strasser, J. S. Kaminker, M. Tessier-Lavigne, Microarray analysis of retinal endothelial tip cells identifies CXCR4 as a mediator of tip cell morphology and branching. *Blood* **115**, 5102–5110 (2010).
28. A. Fantin *et al.*, NRP1 regulates CDC42 activation to promote filopodia formation in endothelial tip cells. *Cell Rep.* **11**, 1577–1590 (2015).
29. A. W. Chung *et al.*, Endothelial dysfunction and compromised eNOS/Akt signaling in the thoracic aorta during the progression of Marfan syndrome. *Br. J. Pharmacol.* **150**, 1075–1083 (2007).
30. J. P. Habashi *et al.*, Angiotensin II type 2 receptor signaling attenuates aortic aneurysm in mice through ERK antagonism. *Science* **332**, 361–365 (2011).
31. T. J. Broekelmann, N. K. Bodmer, R. P. Mecham, Identification of the growth factor-binding sequence in the extracellular matrix protein MAGP-1. *J. Biol. Chem.* **295**, 2687–2697 (2020).
32. A. S. Penner, M. J. Rock, C. M. Kielty, J. M. Shipley, Microfibril-associated glycoprotein-2 interacts with fibrillin-1 and fibrillin-2 suggesting a role for MAGP-2 in elastic fiber assembly. *J. Biol. Chem.* **277**, 35044–35049 (2002).
33. C. S. Craft, T. J. Broekelmann, R. P. Mecham, Microfibril-associated glycoproteins MAGP-1 and MAGP-2 in disease. *Matrix. Biol.* **71–72**, 100–111 (2018).
34. M. Henderson, R. Polewski, J. C. Fanning, M. A. Gibson, Microfibril-associated glycoprotein-1 (MAGP-1) is specifically located on the beads of the beaded-filament structure for fibrillin-containing microfibrils as visualized by the rotary shadowing technique. *J. Histochem. Cytochem.* **44**, 1389–1397 (1996).
35. A. Miyamoto, R. Lau, P. W. Hein, J. M. Shipley, G. Weinmaster, Microfibrillar proteins MAGP-1 and MAGP-2 induce Notch1 extracellular domain dissociation and receptor activation. *J. Biol. Chem.* **281**, 10089–10097 (2006).
36. V. Caolo *et al.*, Feed-forward signaling by membrane-bound ligand receptor circuit: The case of Notch-delta-like 4 ligand in endothelial cells. *J. Biol. Chem.* **285**, 40681–40689 (2010).
37. D. Hubmacher *et al.*, Biogenesis of extracellular microfibrils: Multimerization of the fibrillin-1 C terminus into bead-like structures enables self-assembly. *Proc. Natl. Acad. Sci. U.S.A.* **105**, 6548–6553 (2008).
38. Y. Dong, F. Alonso, T. Jahjah, I. Fremaux, E. Genot, Angiogenesis invasion assay to study endothelial cell invasion and sprouting behavior. *Methods Mol. Biol.* **2608**, 345–364 (2023).
39. Y. Dong *et al.*, miR-155 regulates physiological angiogenesis but an miR-155-rich microenvironment disrupts the process by promoting unproductive endothelial sprouting. *Cell. Mol. Life Sci.* **79**, 208 (2022).
40. S. Z. Karoulias, N. Taye, S. Stanley, D. Hubmacher, The ADAMTS/Fibrillin Connection: Insights into the biological functions of ADAMTS10 and ADAMTS17 and their respective sister proteases. *Biomolecules* **10**, 596 (2020).
41. R. del Toro *et al.*, Identification and functional analysis of endothelial tip cell-enriched genes. *Blood* **116**, 4025–4033 (2010).
42. J. Oller *et al.*, Nitric oxide mediates aortic disease in mice deficient in the metalloprotease Adamts1 and in a mouse model of Marfan syndrome. *Nat. Med.* **23**, 200–212 (2017).
43. Y. Fu *et al.*, Proteolytic cleavage of versican and involvement of ADAMTS-1 in VEGF-A/VPF-induced pathological angiogenesis. *J. Histochem. Cytochem.* **59**, 463–473 (2011).
44. N. V. Lee *et al.*, ADAMTS1 mediates the release of antiangiogenic polypeptides from TSP1 and 2. *EMBO J.* **25**, 5270–5283 (2006).
45. A. M. Abu El-Asrar *et al.*, Differential expression and localization of ADAMTS proteinases in proliferative diabetic retinopathy. *Molecules* **27**, 5977 (2022).
46. Z. Isogai *et al.*, Versican interacts with fibrillin-1 and links extracellular microfibrils to other connective tissue networks. *J. Biol. Chem.* **277**, 4565–4572 (2002).

47. D. Stenzel *et al.*, Endothelial basement membrane limits tip cell formation by inducing Dll4/Notch signalling in vivo. *EMBO Rep.* **12**, 1135–1143 (2011).
48. A. Fantin *et al.*, Neuropilin 1 (NRP1) hypomorphism combined with defective VEGF-A binding reveals novel roles for NRP1 in developmental and pathological angiogenesis. *Development* **141**, 556–562 (2014).
49. M. V. Gelfand *et al.*, Neuropilin-1 functions as a VEGFR2 co-receptor to guide developmental angiogenesis independent of ligand binding. *ELife* **3**, e03720 (2014).
50. S. F. Rocha *et al.*, Esm1 modulates endothelial tip cell behavior and vascular permeability by enhancing VEGF bioavailability. *Circ. Res.* **115**, 581–590 (2014).
51. S. A. Jensen, D. P. Reinhardt, M. A. Gibson, A. S. Weiss, Protein interaction studies of MAGP-1 with tropoelastin and fibrillin-1. *J. Biol. Chem.* **276**, 39661–39666 (2001).
52. A. R. Albig, D. J. Becenti, T. G. Roy, W. P. Schiemann, Microfibril-associate glycoprotein-2 (MAGP-2) promotes angiogenic cell sprouting by blocking notch signaling in endothelial cells. *Microvasc Res.* **76**, 7–14 (2008).
53. R. P. Mecham, M. A. Gibson, The microfibril-associated glycoproteins (MAGPs) and the microfibrillar niche. *Matrix Biol.* **47**, 13–33 (2015).
54. F. Ramirez, L. Y. Sakai, D. B. Rifkin, H. C. Dietz, Extracellular microfibrils in development and disease. *Cell Mol. Life Sci.* **64**, 2437–2446 (2007).
55. K. E. Gregory *et al.*, The prodomain of BMP-7 targets the BMP-7 complex to the extracellular matrix. *J. Biol. Chem.* **280**, 27970–27980 (2005).
56. M. J. Rock *et al.*, Molecular basis of elastic fiber formation. Critical interactions and a tropoelastin-fibrillin-1 cross-link. *J. Biol. Chem.* **279**, 23748–23758 (2004).
57. S. A. Cain, E. J. Mularczyk, M. Singh, T. Massam-Wu, C. M. Kielty, ADAMTS-10 and -6 differentially regulate cell-cell junctions and focal adhesions. *Sci. Rep.* **6**, 35956 (2016).
58. H. Du *et al.*, Macrophage-released ADAMTS1 promotes muscle stem cell activation. *Nat. Commun.* **8**, 669 (2017).
59. Y. Perez-Riverol *et al.*, The PRIDE database and related tools and resources in 2019: Improving support for quantification data. *Nucleic Acids Res.* **47**, D442–D450 (2019).